Korean J. Chem. Eng., 34(4), 1073-1080 (2017)
DOI: 10.1007/s11814-016-0348-3

pISSN: 0256-1115
eISSN: 1975-7220

Acid-hydrolyzed agricultural residue: A potential adsorbent for the decontamination of naphthalene from water bodies

Mijia Zhu†, Wei Tian, Hankui Chai, and Jun Yao

School of Energy & Environmental Engineering, University of Science and Technology Beijing, 100083 Beijing, P. R. China
(*Received 28 August 2016 • accepted 10 December 2016*)

Abstract−Development and application of low-cost and effective adsorbents to remove polycyclic aromatic hydrocarbons from effluents has become a research focus in recent years. We selected reed stem, ginkgo nut shell and hazelnut shell as adsorbents, and used acid hydrolysis as a simple modification technology. The adsorption isotherms of naphthalene to raw and modified adsorbents were controlled by partitioning. The adsorption capability of the hydrolysed hazelnut shell was notably enhanced at a higher level compared with that of other adsorbents. Results showed that the adsorption capacity (17250.42 μg/g) of modified hazelnut shell was observed for an initial naphthalene concentration of 25 mg/L, with a contact time of 72 h, adsorbent dosage of 1 g/L and initial pH of 7.0. Furthermore, the regeneration capability of hydrolyzed hazelnut shell indicated that it was a promising adsorbent for naphthalene removal in wastewater treatment.

Keywords: Polycyclic Aromatic Hydrocarbons, Adsorbents, Acid Hydrolysis, Partitioning, Adsorption Coefficients

INTRODUCTION

Petroleum contamination is a great threat that poses a challenge to environmental protection efforts. Increasing crude oil production and elevated probability of accidents (e.g., extraction, transportation and storage) contribute to the risk of hydrocarbon spillage or leakage [1]. Crude oil is a highly toxic compound consisting of aromatic, aliphatics and polar chemicals [2]. Among the organic components, polycyclic aromatic hydrocarbons (PAHs) have received much attention because of their high persistence in the environment [3]. Contamination by PAHs presents a significant risk to both the local ecosystem and human health. Some researchers have reported that the accumulation of PAHs can cause severe oxidative DNA damage, thereby leading to cancer [4].

In recent years, the widespread occurrence of PAH contamination in the aquatic environment has become a major concern [5-9]. Various methodologies, such as biodegradation, photodegradation, UV irradiation, ozonation, membrane filtration, coagulation and activated carbon adsorption, have been applied to remove PAHs from aqueous solution [8,10]. The biological process is less expensive. The method has been applied in the low molecular weight PAHs degradation. Its drawbacks, however, include long incubation time. Physical and chemical processes may be more efficient in the removal of these substances, but these treatments have many disadvantages, such as high operation cost, corrosion and secondary pollution [11]. As an environmental technology, adsorption has a vital role in greatly reducing the amount of organic contamination in aqueous solution [12,13].

From technical and economic points of view, some natural adsorbents are applied as low-cost sorbent alternatives. They are widely available and renewable. A variety of agricultural materials have been proposed to remove pollutants from aqueous solutions, including cork, bean pods, malt spent rootlets, *sterculia guttata* shell, *Ficus auriculata* leaves and other plant residues [14-19]. Previous research has revealed that sorption of aromatic compounds by adsorbents was significantly influenced by their structural characteristics (e.g., polarity and aromaticity) [16]. Huang et al. found that aspen wood fiber was an effective sorbent for persistent organic pollutant removal. As a major component in the adsorbent, lignin exhibits a positive effect on adsorption capacity, whereas the other two components (cellulose and hemicellulose) limit the affinity of hydrophobic compounds [20]. The differences among the three components were attributed to the surface functional groups. For instance, cellulose and hemicelluloses show strong hydrophilicity because of their polyhydroxyl and polycarboxylic structures. However, the lignin phenylpropane units may have relatively hydrophobic areas for PAH uptake. Xi et al. reported that PAH removal was notably enhanced by de-sugared plant residues [16]. However, more studies on raw and de-sugared adsorbents are needed. To our knowledge, a majority of the published studies on the application of raw and modified adsorbent mainly focused on the structure and surface functional groups [21-23]. Few studies focused on the factors in the aquatic environment.

In the present work we evaluated agricultural wastes as adsorbents for the removal of PAH from effluents. Naphthalene was chosen as the model PAH in the experiment because of its widespread occurrence in wastewater and surface water [24,25]. Reed stem (RS), ginkgo nut shell (GNS) and hazelnut shell (HNS) were chosen as the adsorbents because they are common agricultural by-products and are available in large quantities in the north of China [26-29]. The effect of contact time, adsorbent dosage, solution pH and ionic strength on the PAH adsorption was examined. The ad-

†To whom correspondence should be addressed.
E-mail: zhumijia128@163.com

sorption mechanism and kinetics were exploited, and factors affecting the adsorption capacity of PAH were determined.

MATERIALS AND METHODS

1. Preparation of Adsorbents

Three agricultural residues samples, reed stem (RS), ginkgo nut shell (GNS) and hazelnut shell (HNS), were collected from Hebei Province, China, September 2014. These samples were washed with deionized distilled water. The polysaccharide component was reduced from RS, GNS and HNS using acid hydrolysis, which was mentioned in a previous report [16]. De-sugared reed stem (RS-DS), de-sugared ginkgo nut shell (GNS-DS) and de-sugared hazelnut shell (HNS-DS) were produced after the chemical reaction. After that, they were sieved to less than 0.154 mm. The process can be seen in Fig. 1. The samples (RS, GNS, HNS, RS-DS, GNS-DS and HNS-DS) were characterized by infrared spectroscopy (FTIR) and scanning electron micrograph (SEM). The spectrum was calculated in the range from 4,000 to 400 cm^{-1} using a Perkin Elmer Model spectrum 400 FTIR/FTNIR spectrometer with deuterated triglycine sulfate detector and KBr beam splitter. The samples were dried at room temperature and coated with Au under vacuum in an argon atmosphere for the SEM analysis (SU8010, Hitachi, Tokyo, Japan). The C, H and N contents in the raw and modified adsorbents were calculated by using a Flash EA 1112 CHN elemental analyzer (ThermoFinnigan), whereas the oxygen content was measured by the mass difference. The index of aromaticity and polarity of samples were determined by the atomic ratios of H/C and (O+N)/C. The Brunauer-Emmett-Teller (BET) specific surface area of the samples were calculated by a Beckman Coulter SA3100-type instrument (Beckman Cor. US). The elemental analyses and the specific surface area of the samples are summarized in Table 1.

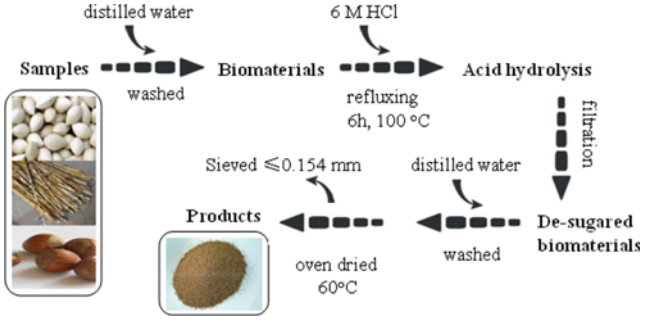

Fig. 1. The de-sugared process of agricultural residues.

2. Preparation of Adsorbate

Adsorption of naphthalene on the raw and de-sugared samples was investigated to elucidate the different capacities of the selected adsorbents. Because of the low water solubility of naphthalene, the methanol-water solution was used as the carrier solution (octanol-water partition coefficients $K_{ow}=1.95\times10^3$). Methanol concentrations were kept less than 0.1% of the total volume of solution to avoid co-solvent effects [16]. The PAH solutions were made by dissolving appropriate amounts of solutes in methanol (HPLC grade) and then diluting with a background solution containing 0.01 mol/L $CaCl_2$ and 200 mg/L NaN_3 (biocide).

3. Batch Adsorption Experiment

Batch adsorption isotherms were obtained by contacting a certain amount of adsorbent with 50mL naphthalene solution of different initial concentrations (0.2-25 mg/L). Each isotherm contained seven concentration points, including the blank sample (containing adsorbent without naphthalene), and each point contained a calibration sample (without adsorbent). These samples were placed in 50 mL screw cap vials and subsequently capped and shaken in a mechanical shaker for 72 h at 200 rpm. The tests involved using triplicate batch experiments. The samples were agitated in the dark condition at room temperature (T=298 K) to reach equilibrium. The same procedures were followed to examine the adsorption parameters (e.g., adsorbent dosage, 0.1-6 g/L; pH, 2-10; ionic strength, 0-1 mol/L).

4. Recycle Test

The recycle experiment of adsorbent, which was used to remove PAH, was conducted in an apparatus that consisted of a stainless-steel reactor (20 cm×20 cm×15 cm) and a furnace (Thermolyne, Zhongtian Inc., China) that could reach a maximum temperature of 600 °C. Pure nitrogen was applied as an inert sweep gas and controlled using a mass flow detector. The adsorbent used for the uptake of PAH was separated from the solution after the adsorption process and then placed in the reactor. To avoid combustion in the recycle process, the residual oxygen was removed by a nitrogen sweep gas at a flow rate of 250 mL/min. Afterwards, the PAH was removed from the adsorbent by increasing the temperature of the recycle unit.

5. Analytic Methods

The concentrations of naphthalene in solution were measured by high-performance liquid chromatography (Agilent 1200 HPLC) with a G1321A fluorescence detector and Agilent Eclipse XDB-C 18 column (4.6 mm×250 mm×5 μm). A 15 μL mobile phase (ace-

Table 1. Elemental and specific surface area analysis of samples

Sample	C (wt%)	H (wt%)	N (wt%)	O* (wt%)	H/C	(O+N)/C	S_{BET} (m^2/g)
RS	46.12	5.87	0.41	47.60	1.53	0.78	338
GNS	47.22	5.93	0.52	46.33	1.51	0.74	272
HNS	49.45	6.21	0.47	43.87	1.50	0.67	379
RS-DS	63.2	5.21	0.32	31.27	0.99	0.38	1200
GNS-DS	63.73	4.82	0.39	31.06	0.91	0.37	1076
HNS-DS	65.51	4.45	0.37	29.67	0.82	0.34	1085

*Oxygen content was calculated by mass difference

tonitrile/water, v/v=9 : 1) was injected with a flow rate of 1 mL/min. The concentrations of naphthalene at equilibrium (C_e) were determined by HPLC at the excitation and emission wavelength of 220 and 325 nm, respectively [16]. To avoid the losses caused by evaporation, biodegradation and adsorption on the wall, the naphthalene adsorption was measured by the concentration difference of sorbate between the calibration and the control. All experimental data was obtained by repeating three times, with the average value of the three measurements being presented.

6. Data Analysis

Removal efficiency (w) and adsorption capacity (Q_e) of adsorbents were calculated in the following equations:

$$w = \frac{C_0 - C_t}{C_0} \times 100\% \quad (1)$$

$$Q_e = \frac{(C_0 - C_e)V}{m} \quad (2)$$

where C_0 and C_t (mg/L) refer to the naphthalene concentrations at initial and instantaneous (at time t), respectively. V (L) is the volume of the bulk solution. m (g) is the adsorbent mass. Q_e (μg/g) represents the amount adsorbed per unit weight of adsorbent. C_e (mg/L) refers to the equilibrium concentration in the aqueous solution.

The adsorption isotherms were fitted using the two most common models (Langmuir and Freundlich). The relative parameters were calculated by linear regression by Origin 8.0. The Langmuir isotherm corresponds to homogeneous adsorption [30], which can be described by the equation:

$$Q_e = \frac{K_L Q_{max} C_e}{1 + K_L C_e} \quad (3)$$

where Q_{max} is the maximum monolayer adsorption capacity (μg/g), and K_L is the affinity constant related to the free energy of adsorption (L/μg).

In comparison to the Langmuir, the Freundlich isotherm is used to describe heterogeneous surface adsorption and multilayer adsorption [31]. The model is shown in the following equation:

$$Q_e = K_F C_e^{1/n} \quad (4)$$

where K_F is the Freundlich index, which indicates the adsorption capacity of the adsorbent [(μg/g)·(L/μg)$^{1/n}$], and n is the Freundlich exponent related to adsorption intensity.

The kinetic study is important for process design and parameter control, and also to provide information on the mechanism of adsorption [18]. Four kinetic models were introduced in the experiments.

The pseudo-first-order kinetics describes the adsorption rate of a solute by the adsorbent depending on biosorption capacity; the model is expressed in Eq. (5):

$$\log(Q_e - Q_t) = \log Q_e - \frac{k_1 t}{2.303} \quad (5)$$

where Q_e (μg/g) and Q_t (μg/g) represent the amounts of naphthalene adsorption at equilibrium and at time t (hr), respectively, and k_1 (hr^{-1}) is the pseudo-first-order rate constant.

The pseudo-second-order describes the relation between mass of the sorbate per unit mass of the adsorbent and contact time; the model is expressed in Eq. (6):

$$\frac{t}{Q_t} = \frac{1}{k_2 Q_e^2} + \frac{t}{Q_e} \quad (6)$$

where k_2 (g/(μg·hr)) is the pseudo second-order rate constant.

The Elovich kinetics model is commonly applied to calculate the adsorption behavior of a process wherein a rapid equilibrium rate is observed in the early period which diminishes gradually in the later period. The equation is expressed in Eq. (7):

$$Q_t = \frac{1}{b}\ln(ab) + \frac{1}{b}\ln t \quad (7)$$

where constants a (μg/(g-hr)) and b (g/μg) represent the initial adsorption rate and surface coverage for chemisorption in the model, respectively [34].

In adsorption systems where there is the possibility of intraparticle diffusion the approach is described as follows:

$$Q_t = K_p t^{1/2} + c \quad (8)$$

where c is a constant which is proportional to the thickness of the boundary layer, the K_p is the slope of straight-line portions of plot of Q_t vs. $t^{1/2}$ [35,36].

RESULTS AND DISCUSSION

1. Characterization of Adsorbents

The FTIR spectra between 4,000 and 450 cm^{-1} for the adsorbents (raw and de-sugared) are presented in Fig. 2. The large band in the region of 3,428 cm^{-1} represents the stretching vibration of the hydroxyl groups. The adsorption bands (1,635 cm^{-1}) were attributed to the aromatic C=C and C=O. The peaks (1,512 cm^{-1}) represent the C=C ring stretching vibration. The peaks of 1,724 cm^{-1} represent the carbonyl stretch of -COOH group. For the raw adsorbents, the peaks at 1,128 cm^{-1} and 1,068 cm^{-1} were assigned to C-O-C stretching vibration. The peaks at 2,920, 2,854 and 1,430 cm^{-1} were ascribed to CH_2 units. Compared to the raw samples, peaks of

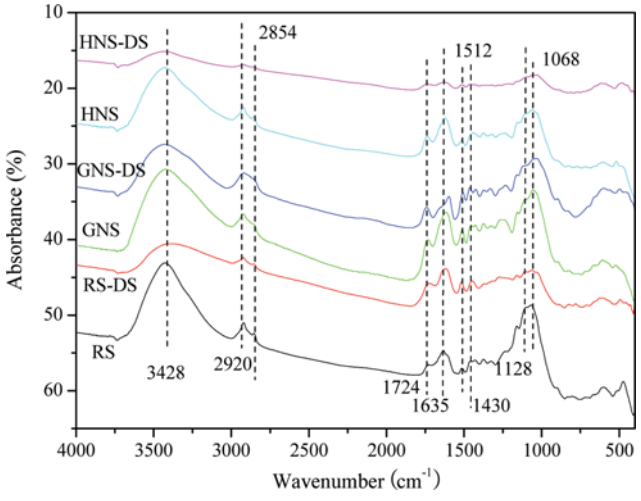

Fig. 2. Fourier transform infrared spectra of the raw and de-sugared adsorbents.

Table 2. Isotherm constants of the models for the adsorption of naphthalene by biomaterials

Sorbent	Linear model		Freundlich model			K_{oc} (L/kg)
	K_d (L/kg)	R^2	n	$logK_F$	R^2	
RS	201.23	0.9987	1.10	2.22	0.9982	436.32
GNS	225.83	0.9998	1.08	2.31	0.9997	478.25
HNS	266.01	0.9896	1.10	2.26	0.9875	537.94
RS-DS	1825.57	0.9774	2.09	2.71	0.9591	2888.56
GNS-DS	1937.64	0.9997	1.33	3.10	0.9967	3040.39
HNS-DS	2345.18	0.9937	1.29	3.19	0.9912	3579.88

-COOH, C=C and CH_2 were significantly enhanced, whereas C-O-C bands were sharply reduced after acid hydrolysis. The insignificant peaks of C-O-C in the de-sugared samples were due to the removal of polysaccharide content in the process of acid hydrolysis. Xi et al. obtained similar findings [16].

Fig. S1 shows the scanning electron micrograph of the raw and acid-hydrolyzed samples. It can be seen that the surface morphologies of the acid-hydrolyzed adsorbents are irregular and porous, which could lead to high uptake of naphthalene. Moreover, the skeleton structure (lignin components) still exists in the acid-hydrolyzed adsorbents.

2. Effect of Adsorbents

The adsorption isotherm is generally used to describe the adsorbate molecules distributed between the liquid phase and the solid phase when the adsorption process reaches an equilibrium state. So it is an important step for the determination of adsorbent capacity. Adsorption isotherms of naphthalene on raw and modified biomaterials are conducted at different initial naphthalene concentration (0.2-25 mg/L). The isotherms fit well with the Freundlich model; the linear and Freundlich regression parameters are listed in Table 2. The Freundlich *n* values ranged from 1.08 to 2.09. The weak nonlinear isotherms indicated that the dominant mechanism for adsorbents was a partition process, probably due to π-π electron interaction between naphthalene molecules and aromatic cores of adsorbents. The hydrophobic moieties interacted with one another, thereby producing a partition medium that renders the sorption of nonpolar organic compounds [37]. Similar phenomena were also observed for PAHs adsorption using plant residue materials, pine bark and others [21,38].

Adsorption coefficients K_d and K_{oc} were also calculated and presented in Table 2, where K_d was calculated from the slope of the linear isotherms, and K_{oc} was obtained by normalizing K_d to the carbon level (f_{oc}, carbon wt%) of each sorbent. K_d is used to describe the adsorption efficiency for organic pollutants [16]. The K_d values of the samples for naphthalene were ranked in the following order: RS (201.23 L/kg)<GNS (225.83 L/kg)<HNS (266.01 L/kg)< RS-DS (1,825.57 L/kg)<GNS-DS (1,937.64 L/kg)<HNS-DS (2,345.18 L/kg). The enhancement in adsorption capacity of adsorbents after surface modification was partly attributed to the removal of the sugar components (e.g., polysaccharides). Previous studies demonstrated that polysaccharides had a negative effect on the uptake of PAHs [16,20,38]. Moreover, the specific surface area was increased after the treatment. From Table 1, the BET surface area of the de-sugared samples ranged from 1,076 m^2/g to 1,200 m^2/g, while those of the oral samples ranged from 272 m^2/g to 379 m^2/g. For the adsorbent, the high specific surface area could lead to the better uptake of naphthalene.

With increasing total organic carbon content, the indexes of polarity dropped significantly, and aromaticity was enhanced notably. As presented in Fig. S2, positive correlation (linear correlation coefficient R^2=0.9975) of K_d values with aromaticity (H/C) for the adsorbents was observed, whereas a negative correlation (R^2=0.9656) between K_d and (O+N)/C ratio was obtained. The K_{oc} values decreased linearly with increasing polarity of the raw and de-sugared biomaterials (R^2=0.9694). Similar trend was also shown in the sorption of PAHs by plant residue [16]. The relationship between the adsorption capacity and characteristics of the sorbent provides several fundamental information to enhance the PAH uptake capacity of adsorbent by modification. Adsorption coefficient (K_d) is a good indicator to measure the partition efficiency with hydrophobic organic compounds. Comparing the adsorption efficiency of various sorbents is of great interest to researchers. Table S1 lists the K_d values of various sorbents, including different kinds of natural and synthetic sorbents. The K_d values for naphthalene in the study are in the range of 201.23 L/kg to 2,345.18 L/kg, which are comparable to several sorbents. Sorption capacity of HNS is higher than that of raw agricultural waste, such as chitin, chitosan and sugarcane bagasse because of its comparable lignin content [23]. After the acid treatment, de-sugared pine needles and de-sugared pine wood show lower ratio of H/C (1.03 and 1.05, respectively), thereby expressing higher aromaticity and strong affinity with non-polar compounds (K_d=1m871-2m124 L/kg), which were still lower than that of HNS-DS (K_d=2,345.18 L/kg) [16,21]. Compared with the former modified adsorbents, HNS-DS exhibited the highest C content and lowest O content. It also displayed the lowest polarity [(O+N)/C=0.34] and the highest aromaticity (H/C=0.82) (Table 1).

Surfactant treatment of bentonite showed outstanding efficiency in PAH removal. The partition coefficient of dodecylpyridinium-Bent, CTMA-Bent and CDMBA-Bent was 1,675, 27,000 and 44,000 L/kg, respectively. Higher adsorption capacity was partly due to the paraffin-type bilayer structure and organo-clay loading of long-chain surfactant [39]. Although the adsorption capacity of raw and hydrolyzed materials is often lower than that of some sorbents, such as zeolite [25] and bentonite [7], these are still promising adsorbents for PAH removal because their operation is simple and they are cost effective.

3. Effect of Contact Time

To investigate the adsorption efficiency of adsorbent with PAHs,

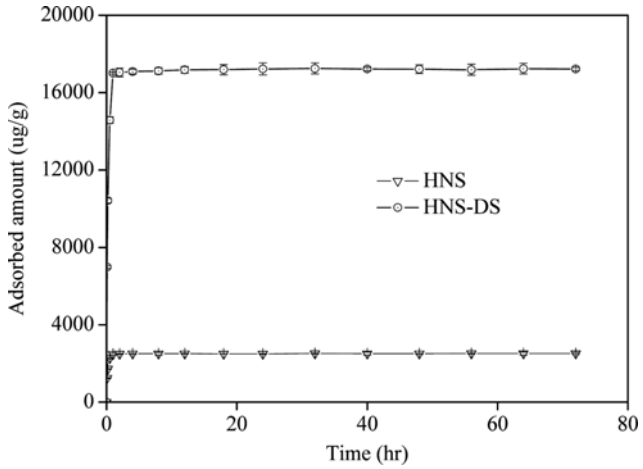

Fig. 3. Dynamic adsorption of HNS and HNS-DS. The bars represent the standard deviation of mean (Conditions: naphthalene concentration 25 mg/L, sorbent dosage 1 g/L, pH 7.0, temperature 298 K).

adsorption kinetics experiments were performed at room temperature (T=298 K) by mixing a measured amount of adsorbent with naphthalene solutions. Fig. 3 depicts the naphthalene adsorption as a function of contact time in using HNS and HNS-DS as adsorbent. Results showed that adsorption efficiency significantly increased with increasing contact time. The adsorption process proceeded at a high rate in the first hour of reaction (for HNS, the extent of adsorption ranged from 0 μg/g to 2,487±15 μg/g; for HNS-DS, the extent of adsorption ranged from 0 μg/g to 1,7012± 225 μg/g) and then became more gradual until equilibrium was achieved after 24 h for HNS and after 48 h for HNS-DS. The equilibrium time for biomaterial adsorption experiments is consistent with that of previous work [16]. The adsorption amounts of naphthalene for HNS and HNS-DS under equilibrium condition were 2,512.00 and 17,250.42 μg/g, respectively.

To better elucidate the mechanism of the adsorption process, Lagergren's pseudo-first-order kinetics, pseudo-second-order kinetics, Elovich model and intraparticle diffusion model were selected to determine the relationship between the amount of adsorbate and reaction time.

The values of kinetic model parameters (Q_e, k_1, k_2, K_P, a, b and c) can be measured using Origin 8.0. The regression results are presented in Table 3. Comparing the values of correlation coefficient of pseudo-first-order, pseudo-second-order and Elovich equations, the pseudo-second-order model is better than the others. Moreover, the calculated equilibrium adsorption capacity ($Q_{e,cal}$) of HNS and HNS-DS for naphthalene based on the pseudo-second-order kinetic model is 2,500.00 and 17,793.59 μg/g, respectively, which is close to the values in the experimental data. All the experiments were conducted under the same conditions except for the adsorbent, which was subjected to a different surface treatment. Higher adsorption performance of acid-hydrolyzed HNS (HNS-DS), compared with that of the raw HNS, verified that the functional groups formed by chemical modification were significant factors that affect the adsorption rate. However, Elovich rate equation was constructed with high values of the correlation coefficients (R^2) for HNS (0.9821) and HNS-DS (0.9955). Compared with the raw HNS, the surface coverage ratio b should have been higher in HNS-DS, because the hydrophobic moieties were increased by acid treatment. This deduction was not consistent with the results, wherein the reported surface coverage ratio b for HNS and HNS-DS was 0.001835 and 0.000228, respectively. Therefore, the Elovich model may not be suitable for describing the kinetics of naphthalene adsorption onto adsorbents.

Table 3. Kinetic parameters for the adsorption of naphthalene by adsorbents (e.g., HNS and HNS-DS) with different models

Models		HNS	HNS-DS
Pseudo-first-order kinetic	k_1	4.3299	4.1543
	$Q_{e,cal}$	1966.47	16248.99
	R^2	0.9987	0.9909
Pseudo-second-order kinetic	k_2	0.004	0.00035
	$Q_{e,cal}$	2500.00	17793.59
	R^2	0.9999	0.9999
Elovich	a	59587.38	227186.68
	b	0.001835	0.000228
	R^2	0.9821	0.9955
Intraparticle diffusion	K_p	1763.4	14323
	C	841.83	3406.2
	R^2	0.9186	0.9512
$Q_{e,exp}$		2512.00	17250.42

4. Effect of Adsorbent Dosage

The effect of adsorbent dosage on the naphthalene removal at an initial concentration of 25 mg/L, contact time of 72 h, pH of 7.0 and temperature of 298 K was determined. From Fig. 4, the naphthalene adsorption of HNS-DS at the dosage of 0.1, 0.25, 0.5, 0.75, 1.0, 1.5, 2.0, 3.0, 4.0 and 6.0 g/L was 18,500±500, 25,200±100, 21,151 ±251, 20,233±467, 17,250±301, 11,917±83, 8,963±25, 5,933±67, 4,469±144 and 2,979±87 μg/g, respectively. Removal efficiency was 7.40±0.2%, 25.2±0.1%, 42.3±0.5%, 60.7±1.4%, 69±1.2%, 71.5± 0.5%, 71.7±0.2%, 71.2±0.8%, 71.5±2.3% and 71.5±2.1%, respectively.

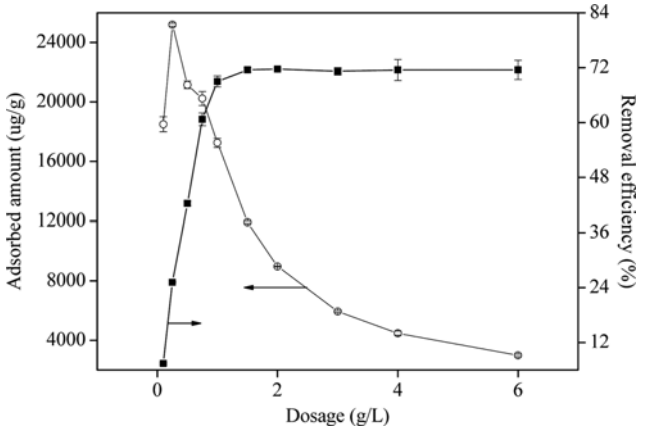

Fig. 4. Effect of dosage on naphthalene adsorption capacity and removal efficiency. The bars represent the standard deviation of mean (Conditions: naphthalene concentration 25 mg/L, pH 7.0, temperature 298 K).

As the adsorbent dosage increased, more binding sites became available, thereby resulting in increased removal efficiency, whereas the decrease in adsorption capacity was due to higher unsaturated adsorption sites [48]. Therefore, based on the removal efficiency of naphthalene and the economics of the process, an adsorbent dosage of 1 g/L was used in the adsorption experiments.

5. Effect of Initial pH

pH is considered as an important parameter in the adsorption process, which can influence the solubility of the adsorbate, and the electrostatic and dispersive interactions between the adsorbent and adsorbate [5]. The effect of pH on the adsorption of naphthalene onto HNS-DS from aqueous solution is illustrated in Fig. 5. The maximum removal efficiency was observed in the range pH 6-8. The removal ratios at pH 6 and 8 were 67.8±0.8% and 68.4±1.9%, respectively. A similar behavior was observed in the adsorption of naphthalene with talc and graphene as sorbents [49,50]. As described in Fig. 6, the adsorption capacity at pH 2 to 4 increased from 14,800±100 μg/g to 15,575±250 μg/g. The adsorption efficiency decreased slightly at pH>8. At lower pH, a huge amount of protons are easily localized onto the adsorbent surface, which significantly decreases the hydrophobic properties of the adsorbent. The surface charge becomes more negative with increasing pH. Thus, the electrostatic interaction between the adsorbent and naphthalene increasingly becomes stronger, thereby overcoming the binding force. The combined effects may be attributed to the slight reduction in the adsorption capacity of adsorbents under alkaline conditions [13].

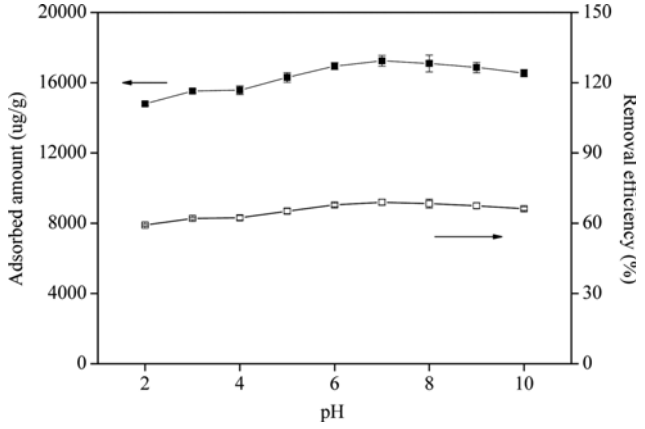

Fig. 5. Effect of pH on naphthalene adsorption capacity and removal efficiency. The bars represent the standard deviation of mean (Conditions: naphthalene concentration 25 mg/L, sorbent dosage 1 g/L, temperature 298 K).

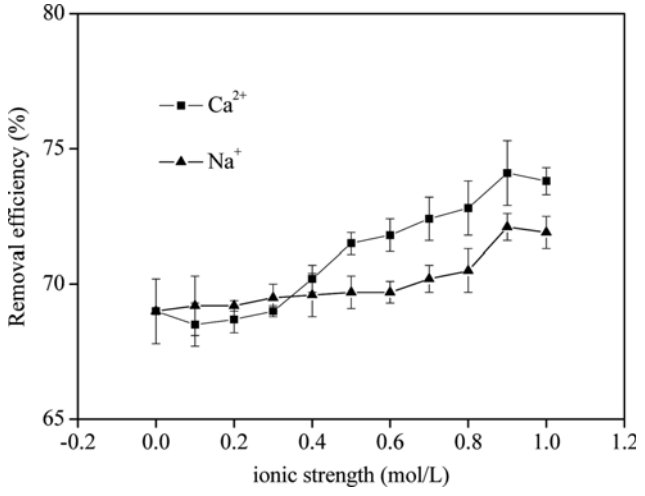

Fig. 6. Effect of ionic strength on naphthalene adsorption capacity and removal efficiency. The bars represent the standard deviation of mean (Conditions: naphthalene concentration 25 mg/L, sorbent dosage 1 g/L, pH 7.0, temperature 298 K).

6. Effect of Ionic Strength

The adsorption of naphthalene onto HNS-DS at different NaCl and $CaCl_2$ concentrations was studied, and the results are shown in Fig. 6. The removal efficiency shows negligible ionic strength-dependence on the electrolyte concentrations. There was a slight increase in naphthalene removal efficiency from 69±1.2% to 73.8±0.5% for Ca^{2+} and from 69±1.2% to 71.9±0.6% for Na^+ when ionic strength increased from 0 mol/L to 1.0 mol/L. These results indicate that the naphthalene adsorption capacity, which was improved by adding Ca^{2+} and Na^+, is limited. The performance of Ca^{2+} is more significant than that of Na^+ because of its stronger ionic strength. Similar phenomenon was also found in the organic compound adsorption [13]. The slight increase in naphthalene adsorption is attributed to the following reasons. First, metal cations (e.g., Ca^{2+} and Na^+) react with the negatively charged group from the surface of the adsorbent, thereby reducing the repulsion between naphthalene and adsorbent. Secondly, the elevated electrolyte in the solution interacts more strongly with water molecules than naphthalene-water interaction, thereby reducing the solubility of the aqueous naphthalene and forcing the naphthalene to adhere to the surface of the adsorbent [51]. As described in the plot, the decline in the removal efficiency while the ionic strength achieved 1.0 mol/L may be due to the fact that Na^+ and Ca^{2+} have occupied the active sites [52].

7. Adsorbent Regeneration

To make the adsorption process more effective, adsorbent regeneration should be tested. The regeneration of HNS-DS was at 300 °C, 400 °C, 500 °C and 600 °C for 2 h in the recycle unit. The recycle test was repeated twice. The regeneration efficiency can be calculated in terms of the following equation:

$$W_r(\%) = \frac{Q_n}{Q_1} \quad (9)$$

where W_r is the regeneration efficiency. Q_1 (μg/g) and Q_n (μg/g) are adsorbed amounts of naphthalene in the first and nth cycles, respectively. The regeneration efficiency achieved was 96.5%±0.2%; 97%±0.1%; 96.8%±0.2% and 97.5%±0.1% over five cycles. Therefore, higher temperature is effective for attaining better regeneration efficiency. The results also suggested that HNS-DS is very promising for naphthalene adsorption.

CONCLUSION

This study focused on the adsorption of naphthalene from an aqueous solution using raw and acid-hydrolyzed agricultural resi-

due. The adsorption isotherms fit well with the Freundlich model. Polarity and aromaticity had significant effects on the adsorption capacity of adsorbents. Positive correlation of partition coefficients with aromaticity, negative correlation between partition coefficients and polarity was observed in the batch adsorption experiments. The acid-hydrolyzed HNS was assumed to be a promising adsorbent for naphthalene in the aqueous solution based on its high adsorption capacity (17,250.42 μg/g) and regeneration efficiency (96.5% ±0.2%-97.5%±0.1%).

ACKNOWLEDGEMENTS

This work is supported in part by grants from the International Joint Key Project from Chinese Ministry of Science and Technology (2010DFB23160), National Natural Science Foundation of China (41273092), Public welfare project of Chinese Ministry of Environmental Protection (201409042).

ABBREVIATION AND SYMBOLS

PAHs : polycyclic aromatic hydrocarbons
RS : reed stem
GNS : ginkgo nut shell
HNS : hazelnut shell
RS-DS : de-sugared reed stem
GNS-DS : de-sugared ginkgo nut shell
HNS-DS : de-sugared hazelnut shell
K_L : affinity constant related to the free energy of adsorption [L/μg]
K_F : Freundlich index $[(\mu g/g)\cdot(L/\mu g)^{1/n}]$
n : Freundlich exponent related to adsorption intensity
K_d : adsorption coefficient [L/kg]
K_{oc} : adsorption coefficient related to the carbon content of adsorbent [L/kg]
a : initial adsorption rate [μg/(g-hr)]
b : surface coverage for chemisorption [g/μg]
c : intraparticle diffusion model constant
K_p : slope ratio of intraparticle diffusion model
W_r : regeneration efficiency [%]
k_1 : pseudo-first-order rate constant $[hr^{-1}]$
k_2 : pseudo-second-order rate constant [g/(μg·hr)]

SUPPORTING INFORMATION

Additional information as noted in the text. This information is available via the Internet at http://www.springer.com/chemistry/journal/11814.

REFERENCES

1. V. Kavitha, A. B. Mandal and A. Gnanamani, *Int. Biodeter. Biodegr.*, **94**, 24 (2014).
2. M. Kim, S. H. Hong, J. Won, U. H. Yim, J. H. Jung, S. Y. Ha, J. G. An, C. Joo, E. Kim, G. M. Han, S. Baek, H. W. Choi and W. J. Shim, *Water Res.*, **47**(2), 758 (2013).
3. W. Yang, Y. H. Lang, J. Bai and Z. Y. Li, *Ecol. Eng.*, **74**, 117 (2015).
4. J. Lee, S. W. Chun, H. J. Kang and F. Talke, *Macromol. Res.*, **19**(6), 582 (2011).
5. Q. Shi, A. Li, Z. Zhu and B. Liu, *J. Environ. Sci.*, **25**(1), 188 (2013).
6. M. Anbia and S. E. Moradi, *Chem. Eng. J.*, **148**(2-3), 452 (2009).
7. S. Changchaivong and S. Khaodhiar, *Appl. Clay Sci.*, **43**(3-4), 317 (2009).
8. R. J. Krupadam, M. S. Khan and S. R. Wate, *Water Res.*, **44**(3), 681 (2010).
9. A. Rubio-Clemente, R. A. Torres-Palma and G. A. Peñuela, *Sci. Total Environ.*, **478**, 201 (2014).
10. X. Xia, G. Li, Z. Yang, Y. Chen and G. H. Huang, *Environ. Pollut.*, **157**(4), 1352 (2009).
11. C. Sakulthaew, S. Comfort, C. Chokejaroenrat, C. Harris and X. Li, *Chemosphere*, **117**, 1 (2014).
12. Z. C. Zeledón-Toruño, C. Lao-Luque, F. X. C. de las Heras and M. Sole-Sardans, *Chemosphere*, **67**(3), 505 (2007).
13. Y. Zhou, P. Lu and J. Lu, *Carbohyd. Polym.*, **88**(2), 502 (2012).
14. M. À. Olivella, P. Jové, A. Bianchi, C. Bazzicalupi and L. Cano, *Chemosphere*, **90**(6), 1939 (2013).
15. B. Cabal, T. Budinova, C. O. Ania, B. Tsyntsarski, J. B. Parra and B. Petrova, *J. Hazard. Mater.*, **161**(2-3), 1150 (2009).
16. Z. Xi and B. Chen, *J. Environ. Sci.*, **26**(4), 737 (2014).
17. S. Valili, G. Siavalas, H. K. Karapanagioti, I. D. Manariotis and K. Christanis, *J. Environ. Manage.*, **128**, 252 (2013).
18. S. Rangabhashiyam, E. Nakkeeran, N. Anu and N. Selvaraju, *Res. Chem. Intermed.*, **41**, 8405 (2015).
19. S. Rangabhashiyam and N. Selvaraju, *J. Mol. Liq.*, **207**, 39 (2015).
20. L. Huang, T. B. Boving and B. Xing, *Environ. Sci. Technol.*, **40**(10), 3279 (2006).
21. B. Chen, M. Yuan and H. Liu, *J. Hazard. Mater.*, **188**(1-3), 436 (2011).
22. B. Chen and M. Yuan, *J. Soils Sediment.*, **11**(1), 62 (2011).
23. R. Crisafully, M. A. L. Milhome, R. M. Cavalcante, E. R. Silveira, D. De Keukeleire and R. F. Nascimento, *Bioresour. Technol.*, **99**(10), 4515 (2008).
24. C. O. Ania, B. Cabal, C. Pevida, A. Arenillas, J. B. Parra, F. Rubiera and J. J. Pis, *Appl. Surf. Sci.*, **253**(13), 5741 (2007).
25. C. F. Chang, C. Y. Chang, K. H. Chen, W. T. Tsai, J. L. Shie and Y. H. Chen, *J. Colloid Interf. Sci.*, **277**(1), 29 (2004).
26. S. Baidas, B. Gao and X. Meng, *J. Hazard. Mater.*, **189**(1-2), 54 (2011).
27. M. Miao, H. Jiang, B. Jiang, S. W. Cui, Z. Jin and T. Zhang, *Food Res. Int.*, **49**(1), 303 (2012).
28. J. Liu, Y. Cheng, C. Liu, C. Zhang and Z. Wang, *Sci. Hortic-Amsterdam*, **150**, 348 (2013).
29. J. Liu, Y. Cheng, K. Yan, Q. Liu and Z. Wang, *Sci. Hortic-Amsterdam*, **136**, 128 (2012).
30. I. Langmuir, *J. Am. Chem. Soc.*, **40**, 1361 (1918).
31. H. Freundlich, Methuen, London, UK (1926).
32. S. Lagergren, *Handlingar*, **24**, 1 (1898).
33. Y. S. Ho and G. Mckay, *Process Biochem.*, **34**, 451 (1999).
34. J. S. Cao, J. X. Lin, F. Fang, M. T. Zhang and Z. R. Hu, *Bioresour. Technol.*, **163**, 199 (2014).
35. C. K. Jain and M. K. Sharma, *Water Air Soil Pollut.*, **137**(1-4), 1 (2002).
36. M. YalÇin, A. GÜrses, Ç. Doğar and M. SÖZbİLİr, *Adsorption*,

10(4), 339 (2005).
37. S. S. Banerjee, M. V. Joshi and R. V. Jayaram, *Chemosphere*, **64**(6), 1026 (2006).
38. Y. Li, B. Chen and L. Zhu, *Bioresour. Technol.*, **101**(19), 7307 (2010).
39. L. Xu, M. Zhang and L. Zhu, *Appl. Clay Sci.*, **100**, 29 (2014).
40. M. Novoszad, M. H. Gerzabek, G. Haberhauer, M. Jakusch, H. Lischka, D. Tunega and H. Kirchmann, *Chemosphere*, **59**(5), 639 (2005).
41. B. E. Whitman, J. R. Mihelcic and D. R. Lueking, *Appl. Microbiol. Biot.*, **43**(3), 539 (1995).
42. W. Yang, D. Lampert, N. Zhao, D. Reible and W. Chen, *J. Soils Sediment.*, **12**(5), 713 (2012).
43. M. G. R. Vianna, J. Dweck, F. Quina, F. S. Carvalho and C. O. Nascimento, *J. Therm. Anal. Calorim.*, **100**(3), 889 (2010).
44. X. Shen, X. Wang, S. Tao and B. Xing, *Environ. Sci. Pollut. Res.*, **21**(20), 11979 (2014).
45. X. Cheng, A. Kan and M. Tomson, *J. Nanopart. Res.*, **7**(4-5), 555 (2005).
46. S. Y. Lee and S. J. Kim, *Appl. Clay Sci.*, **22**(1-2), 55 (2002).
47. X. Ruan, P. Sun, X. Ouyang and G. Qian, *Chinese Sci. Bull.*, **56**(32), 3431 (2011).
48. S. Ibrahim, S. Wang and H. M. Ang, *Biochem. Eng. J.*, **49**(1), 78 (2010).
49. S. Şener and A. Özyılmaz, *Ultrason. Sonochem.*, **17**(5), 932 (2010).
50. X. Yang, J. Li, T. Wen, X. Ren, Y. Huang and X. Wang, *Colloids Surf., A: Physicochemical and Engineering Aspects*, **422**, 118 (2013).
51. M. K. Chung, M. T. K. Tsui, K. C. Cheung, N. F. Y. Tam and M. H. Wong, *Sep. Purif. Technol.*, **54**(3), 355 (2007).
52. G. Liu, J. Ma, X. Li and Q. Qin, *J. Hazard. Mater.*, **164**(2), 1275 (2009).